Morphology-Dependent Anomalous Frequency Shifts of Infrared Absorption Bands: Poly(tetrafluoroethylene) and Its Linear Oligomers Perfluoroeicosane and Perfluorotetracosane

Masamichi Kobayashi,* Mami Sakashita, and Toshihisa Adachi

Department of Macromolecular Science, Faculty of Science, Osaka University, Toyonaka, Osaka 560, Japan

Mitsue Kobayashi

Research Reactor Institute, Kyoto University, Sennan, Osaka 590-04, Japan

Received February 28, 1994; Revised Manuscript Received September 13, 1994[⊗]

ABSTRACT: Morphology-dependent frequency shifts of the infrared parallel bands of poly(tetrafluoroethylene) (PTFE) were investigated using a PTFE sample having a whisker-like crystal morphology and lamellar crystals of linear oligomers of PTFE (perfluoro-*n*-eicosane ($C_{20}F_{42}$) and perfluoro-*n*-tetracosane ($C_{24}F_{50}$)). The vibrational assignments of the infrared-active zone-center fundamentals were established through polarization measurements on well-oriented thin films of PTFE and thin layers of $C_{20}F_{42}$ deposited on a metal surface. Based on the assignments thus decided, it has been demonstrated that the A_2 bands with the transition dipoles parallel to the chain axis are blue-shifted as the crystal morphology of the sample goes from the extended-chain crystal to the lamellar crystal, whereas the E_1 perpendicular bands as well as the infrared-inactive Raman bands (the A_1 and E_2 bands) remain unshifted. The magnitudes of the frequency shifts of the A_2 bands were interpreted quantitatively in terms of the transition dipolar coupling theory. The role of the in-phase oscillation of the parallel transition dipoles in this spectral phenomenon was investigated by the analysis of the frequency shifts of the parallel progression bands of the oligomers in their lamellar type mixed crystals of various compositions.

Introduction

In crystalline solids of linear high polymers, the crystallites assume various types of morphologies situated in between the two extreme cases of the fully extended-chain crystal (ECC) and the folded-chain or lamellar crystal (FCC), depending on the crystallization conditions as well as the thermal and mechanical histories of the samples. Physical properties of bulk crystalline polymers are strongly influenced by higher order structures like crystal morphology and, therefore, control and characterization of the morphological structures are of importance in the manufacture of high-performance polymeric materials.

The studies in this field have been done mainly by electron microscopy and small-angle X-ray and neutron scattering. On the contrary, it has been believed that vibrational spectroscopy in the mid-infrared region is not informative, or even useless, for studies in this area. However, in the past decade, the present authors and co-workers have demonstrated that for some crystalline polymers including poly(oxymethylene) (both the stable trigonal and metastable orthorhombic forms) (POM)[1−5] and poly(ethylene oxide) (PEO),[6,7] very remarkable infrared spectral changes are induced by change in crystal morphology, even when the unit cell structure and the degree of crystallinity remain unchanged.

The spectral changes are very specific and have the following common features. (1) As the crystal morphology goes from the typical ECC to the lamellar type, only the infrared bands with the transition moments parallel to the chain axis (the infrared parallel bands) are shifted always toward the high-frequency side. (2) The magnitudes of the frequency shifts are proportional to the oscillator strengths of the bands. (3) The infrared bands with the transition moments perpendicular to the chain axis (the infrared perpendicular bands) as well as the infrared-inactive Raman bands remain unshifted. (4) Even for samples that are in highly crystalline states, the intense parallel bands that exhibit large frequency shifts have rather broadened absorption profiles, in contrast to the sharp Lorentzian profiles of the perpendicular bands and the infrared-inactive Raman bands. (5) The absorption profiles of the parallel bands exhibit substantial changes on thermal and/or mechanical sample processings.

These characteristics of the morphology-dependent spectral changes found in POM and PEO were interpreted quantitatively in terms of the transition dipolar coupling theory.[8] The theory demonstrates that the anomalously large high-frequency shifts of the infrared parallel bands in lamellar crystals are attributed to the strong interactions caused by the in-phase oscillation of the parallel transition dipoles distributed in one crystallite having a particular morphology. The strength of such dipolar interactions depends on the morphology of the crystallites; it vanishes for the ideal ECC and gets stronger as the crystallite goes to the lamellar type, giving rise to high-frequency shifts of the parallel bands in proportion to their oscillator strengths. The magnitudes of the band shifts depend also on the lateral packing of the polymer molecules; the smaller the intermolecular distance, the greater is the band shift. Therefore, we are able to anticipate that the morphology-dependent spectral changes are detectable for such crystalline polymers that exhibit intense infrared parallel bands and have a tight helical form carrying no bulky pendant groups.

According to this consideration, we chose poly(tetrafluoroethylene), $(CF_2)_n$ (PTFE), as the next polymer to be examined, because it satisfies the above-mentioned geometric condition and gives rise to medium intense infrared parallel bands.

[⊗] Abstract published in *Advance ACS Abstracts*, December 1, 1994.

0024-9297/95/2228-0316$09.00/0

The present paper deals with the morphology-dependent infrared spectral changes of PTFE. As an ECC type PTFE, we chose a sample generated by an emulsion polymerization, since Folda et al.[9] reported that rodlike whiskers of PTFE were prepared by this method. As the typical lamellar crystals we chose polycrystalline and single-crystal samples of perfluoro-*n*-eicosane ($C_{20}F_{42}$) and perfluoro-*n*-tetracosane ($C_{24}F_{50}$), i.e., linear oligomers of PTFE. These oligomers appear in three crystal modifications at atmospheric pressure, referred to, from higher to lower temperature, as the R (rhombohedral), I (intermediate), and M (monoclinic) phases.[10] In all modifications the molecules assume essentially the same conformation corresponding to the (15/7) uniform helix (the identity period along the polymer chain consists of 15 CF_2 groups arranged in 7 turns of a helix) of PTFE. The observed infrared spectral changes caused by the change in crystal morphology are analyzed quantitatively according to the transition dipolar coupling theory. The role of the in-phase oscillation of the parallel transition dipoles in this phenomenon is investigated by the analysis of the frequency shifts of the parallel progression bands observed in the lamellar-type mixed crystals of $C_{20}F_{42}$ and $C_{24}F_{50}$. Contrary to the zone-center modes of high molecular weight PTFE, the frequencies of the progression bands of the oligomers depend on the chain length; therefore, the in-phase oscillation of the molecules is destroyed in the mixed crystals, so that the high-frequency shifts of the parallel progression bands occurring in lamellar crystals of the respective pure oligomers are anticipated to be reduced in the mixed crystals, and the extent of the reduction might depend on the composition. If this prediction is confirmed experimentally, we have conclusive evidence supporting the transition dipolar coupling mechanism as the origin of the morphology-dependent infrared band shifts.

Experimental Section

A. Samples. A powder sample of PTFE produced by an emulsion polymerization of tetrafluoroethylene was supplied by Daikin Industrial Ltd. This sample had a whisker-like morphology under the view field of the electron microscope as reported in ref 9 and was used as the standard for the ECC sample of PTFE. A highly oriented thin film was prepared by the friction transfer technique.[11,12] A commercial PTFE rod was rubbed on a polished face of a steel block kept at 200 °C. The very thin film formed on the metal surface was transferred onto a KBr plate to be subjected to the IR measurement to ensure infrared polarization of very intense absorption bands. Perfluoro-*n*-eicosane and perfluoro-*n*-tetracosane were purchased from Ardrich Chemical Co. Inc. Thin plate-shaped single crystals of these oligomers were grown from trichlorotrifluoroethane solutions. Mixed crystals of $C_{20}F_{42}$ and $C_{24}F_{50}$ were prepared by melting a powder mixture at 230 °C in a sealed aluminum pan followed by cooling to room temperature.

B. Spectral Measurements. Infrared spectra were taken using a JASCO Fourier transform/infrared (FT/IR) 8300 spectrometer. For the measurements at low temperatures down to 30 K, an Oxford flow-type cryostat was used. The infrared RAS (reflection–absorption spectrum) was measured at room temperature on a thin film of $C_{20}F_{42}$ deposited on the flat surface of an aluminum plate. Transmission spectra of $C_{20}F_{42}$ and $C_{24}F_{50}$ were taken on plate-shaped single crystals so oriented that the basal normal (parallel to the molecular axes) was inclined by various angles of 0–40° to the incidence direction of the IR radiation. For IR measurements on very tiny specimens, a microfocus FT/IR spectrmeter (JASCO Janssen) was used. Raman spectra were measured using a JASCO NR1000 double monochromator with 514.5 nm light from an Ar+ laser for excitation.

Reconsideration of the Vibrational Assignments of PTFE

At atmospheric pressure, PTFE exists in three crystal modifications with solid-state transitions at 19 and 30 °C. The crystal structures were investigated by many authors in the 1950s and 1960s.[13–16] Although there still exist some unsettled problems about the details of the molecular structure in the respective modifications, the molecular conformation of PTFE is now recognized as follows. Below 19 °C the molecules assume a (13/6) uniform helix forming a monoclinic or triclinic lattice. Between 19 and 30 °C the conformation changes to a (15/7) helix, the molecules being arranged in a trigonal lattice. Above 30 °C the molecules are believed to contain some conformational defects even though the hexagonal parallel alignment of the molecules is maintained as a whole.

The zone-center normal modes of the (13/6) uniform helix of PTFE are classified into eight symmetry species ($\Gamma = 4A_1 + 3A_2 + 8E_1 + 9E_2 + ... + 9E_6$), and those of the (15/7) uniform helix are classified into nine species ($\Gamma = 4A_1 + 3A_2 + 8E_1 + 9E_2 + ... + 9E_7$). In both cases the A_1 and E_2 species are Raman-active, the A_2 is IR-active giving rise to parallel absorption bands, the E_1 is active in both IR (perpendicular bands) and Raman spectra, and the other species are optically inactive. Thus, the number of fundamental modes and polarizations expected to be observed in IR and Raman spectra are the same in the two helices.

Vibrational assignments of the IR- and/or Raman-active fundamentals have been investigated by many authors. However, for some IR and Raman bands the assignments still remain unsettled. The most conspicuous feature of the IR spectrum of PTFE is the appearance of very intense absorptions with three peaks at 1242, 1210, and 1150 cm^{-1}. These three bands have differently been assigned by previous authors. The main reason that makes the decision of the symmetry species of these bands difficult is the difficulty in preparing very thin and well-oriented film specimens suitable for IR polarization measurement.

For our purpose, correct assignment of the IR-active A_2 modes is of essential importance, so that we have to start with the establishment of the vibrational assignments of the IR bands of PTFE based on polarization measurements. In what follows, the IR-active fundamentals are designated as $A_2(m)$ ($m = 1-3$) and $E_1(m)$ ($m = 1-8$), the numbering m being made in the order of higher to lower frequency.

The $A_2(1)$ mode [the CF_2 antisymmetric stretch: $\nu_a(CF_2)$] was assigned first by Liang and Krimm[17] to the very weak IR absorption at 1450 cm^{-1}. The three intense IR bands around 1200 cm^{-1} were assigned to the $E_1(1)$ through $E_3(3)$ fundamentals. Thereafter, the $A_2(1)$ mode was assigned by Moynihan to the intense 1210 cm^{-1} band on the basis of IR polarization observed for overtones and combinations.[18] Hannon et al. presented dispersion cuvers for the (15/7) helix obtained by the normal mode calculation based on the Liang–Krimm (L–K) assignment.[19]

The L–K assignment was also supported by Piseri et al.[20] through comparison between the calculated and experimentally obtained dispersion curves for the (15/7) helix along the *c*-axis (by means of coherent neutron inelastic scattering with the aid of IR and Raman data). On the contrary, Boerio and Koenig[21] adopted the Moynihan assignment on the basis of the fact that there were no distinct IR absorptions around 1450 cm^{-1} in

the spectra of a series of PTFE oligomers. They recalculated the dispersion curves based on the assignment and obtained results somewhat different from those in ref 19.

For checking the reliability of the calculated dispersion curves, the spectral data of the progression bands obtained for linear oligomers play important roles. In considering molecular vibrations of the oligomer C_nF_{2n+2} in accordance with the model of simply coupled oscillators, the phase angles ϕ_k between the neighboring CF_2 oscillators allowed for the kth modes on a dispersion curve are given by the equation

$$\phi_k = k\pi/(n-1), \quad k = 1, 2, ..., n-1 \qquad (1)$$

All the vibrational modes with these phase angles are potentially active in the IR and/or Raman spectrum and observed as a series of progression bands in a particular frequency range characteristic of the respective dispersion curve (or branch) of the infinitely long polymer molecule. In the case of PTFE, there are nine branches ν_1 through ν_9, being designated from higher to lower frequency range.

Rabolt and Fanconi[22] compared the frequency data of the Raman progression bands obtained for C_nF_{2n+2} oligomers with the calculated dispersion curves presented by various research groups and claimed that the data points fitted more accurately to the ν_3 branch calculated by Boerio and Koenig (B–K)[21] rather than that presented in ref 20. In a recent work on the IR spectra of PTFE oligomers reported by Hsu et al., the Moynihan assignment and the B–K dispersion curves were adopted.[23]

According to the transition dipolar coupling theory presented by the present authors,[8] the morphology-dependent frequency shift should occur only for the IR-active parallel fundamentals and its magnitude should be proportional to the oscillator strength of the band. If the intense 1210 cm^{-1} band observed commonly in various PTFE samples including the emulsion-polymerized whiskers is assigned to the $A_2(1)$ mode, we predict that the band exhibits a very large blue shift (by 100 cm^{-1} or more estimated from the absorption intensity of the band and the crystal structure of PTFE) in lamellar crystals of the oligomers. Contrary to the prediction, the 1210 cm^{-1} band and the two intense bands at both sides of it as well do not show any noticeable frequncy shift.

This discrepancy motivated us to reexamine the assignments of the three intense IR bands around the 1200 cm^{-1} band through direct polarization measurement on highly oriented samples. For this purpose we used the following samples. First, we prepared a very thin and highly oriented PTFE film by the friction transfer technique (see Experimental Section). With this sample we obtained highly polarized transmission spectra free from saturation of the intense bands (Figure 1). Here, we used a microfocus FT-IR spectrometer because of the small size of this sample. The three intense bands at 1250, 1206, and 1151 cm^{-1} show undoubtedly perpendicular polarization, indicating that they should be assigned, respectively, to the $E_1(1)$, $E_1(2)$, and $E_1(3)$ fundamentals. In contrast, the $A_2(2)$ doublet around 645 cm^{-1} (see the next section) shows clear parallel polarization. The $A_2(3)$ band at 531 cm^{-1} could not be measured with the MCT detector used for the microfocus measurement. Second, a hexagon-shaped lamellar single crystal of $C_{20}F_{42}$ (with thickness

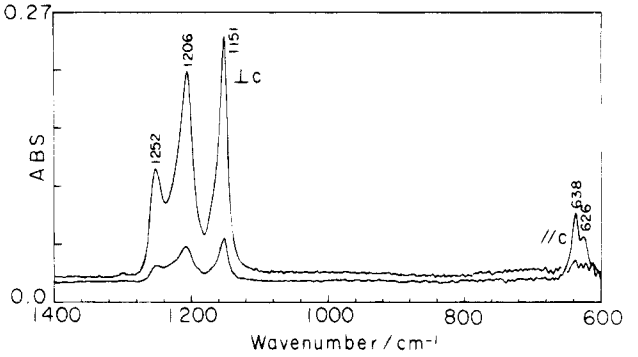

Figure 1. Polarized infrared spectra of PTFE taken on a well-oriented thin film prepared by rubbing a PTFE rod on a steel plate kept at 200 °C.

of ca. 30 μm) was subjected to a transmission spectral measurement.

The polymorphic structures of this compound have been studied by Schwickert et al.[10] At atmospheric pressure there are three crystal modifications which appear in the following temperature ranges: the R (rhombohedral) phase, $T_m = 437\ K \geq T \geq T_{c1} = 200\ K$; the I (intermediate) phase, $T_{c1} \geq T \geq T_{c2} = 143\ K$; and the M (monoclinic) phase, $T < T_{c2}$. In these modifications, the molecules assume essentially the same conformation that corresponds to the (15/7) uniform helix of PTFE in the trigonal form (in the temperature range 19–30 °C). The X-ray diffraction taken on the $C_{20}F_{42}$ single crystal in a wide temperature range covering the appearance of the three modifications showed that the molecular axes are always arranged normal to the lamellar face. The unit cell of the R phase (with the cell dimensions of $a = b = 0.57$ nm, $c = 8.50$ nm, and $\gamma = 120°$) consists of three molecular layers stacked along the c-axis, and each layer contains one molecule per unit cell. The lateral packing of the molecules is essentially the same as that in the trigonal PTFE having the unit cell dimensions of $a = b = 0.566$ nm, $c = 1.69$ nm, and $\gamma = 120°$. The unit cell of the M phase (with the cell dimensions of $a = 0.965$ nm, $b = 0.566$ nm, $c = 1.95$ nm, and $\beta = 97°$) consists of one molecular layer containing two molecules. The molecules are packed in a pseudohexagonal lattice as in the R phase, but handedness of the molecules differs from the case of the R phase; one molecule in the unit cell is a left-handed helix and the other is a right-handed helix.

In the transmission spectrum taken on the single crystal of $C_{20}F_{42}$ at room temperature (the R phase) with the unpolarized IR beam incident normal to the lamellar face, only the perpendicular bands are observed as shown in Figure 2a. The three intense bands around 1200 cm^{-1} are fully saturated and the medium intense band at 555 cm^{-1} associated with the $E_1(4)$ mode [precisely speaking, the most-in-phase mode nearest to the $E_1(4)$ zone-center mode of PTFE] is observed along with very weak perpendicular components of the progression bands (see below).

As the third sample, a thin film of $C_{20}F_{42}$ deposited on an aluminum plate was subjected to reflection–absorption spectroscopy (RAS), where only the modes with transition moment perpendicular to the metal face are excited. As shown in Figure 2b, several weak absorptions are observed in the 1300–1100 cm^{-1} range instead of the three intense bands seen in Figure 2a. The $E_1(4)$ band at 555 cm^{-1} disappears, while the $A_2(2)$ doublet around 645 cm^{-1} and the $A_2(3)$ band at 531 cm^{-1} appear with strong intensities. There are many pro-

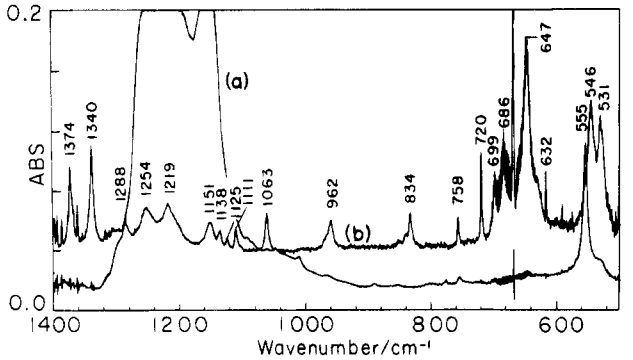

Figure 2. Infrared spectra of $C_{20}F_{42}$ crystals at room temperature: (a) transmission spectrum taken on a lamellar single crystal with normally incident radiation; (b) RAS of a thin film deposited on the flat face of an aluminum plate.

gression bands observed in the frequency range 1400–500 cm^{-1}. Polarizations of the progression bands were decided by the oblique transmission technique. A thin plate of $C_{20}F_{42}$ single crystal was so mounted on the sample holder that the basal normal made an angle θ with the incident beam, and absorption spectra were recorded at various inclination angles. At $\theta = 0$ (normal incidence), only the perpendicular bands were observed as in Figure 2a. With increasing θ, the parallel bands began to appear and got stronger. Figure 3 shows the spectra measured at 110 K (the M phase) with the inclination angle of θ = 0 and 23° (corrected for the refractive index of the sample). Here, the assignments of the ν_2, ν_3, and ν_4 progression bands are described. The progression bands with k = even are strongly polarized parallel to the molecular axis, and some of the odd-numbered modes appear as very weak bands. As far as the polarization is concerned, the same results were obtained at room temperature (the R phase). The spectral data are summarized in Table 1 along with the assignments of the bands. The frequencies of the bands observed in RAS are also given for comparison.

On referring to these spectral data, conformation and orientation of the $C_{20}F_{42}$ molecules in the thin film deposited on the aluminum plate were considered, since the spectral feature of the progression bands reflects more sensitively the state of the molecules than the bands due to the zone-center modes. All the progression bands appearing in RAS in the 1400–1200 and 1125–500 cm^{-1} ranges coincide in both frequency and relative intensity with the parallel progression bands of the single crystal. The weak satellite bands at the high-frequency wings of the $\nu_3(4)$ and $\nu_3(6)$ progression bands observed in both RAS and the transmission spectrum at room temperature (see Figure 5) are associated with the molecules having conformational defects at the chain ends. In bulk samples they decrease in intensity with decreasing temperature and disappear as the sample transforms to the I phase. Details of the IR and Raman spectral changes on solid-state transitions will be reported elsewhere.

The similarity in the spectral pattern of the IR parallel bands of $C_{20}F_{42}$ between the single crystal and the thin film deposited on the metal face, along with the selective appearance of the parallel bands in RAS, suggests that at room temperature the thin film assumes a structure very close to the R phase with the molecules arranged normal to the metal face.

As for the assignment of the weak bands at 1254, 1219, and 1151 cm^{-1} in RAS, there are two possibilities: (1) they are regarded as residues of the very

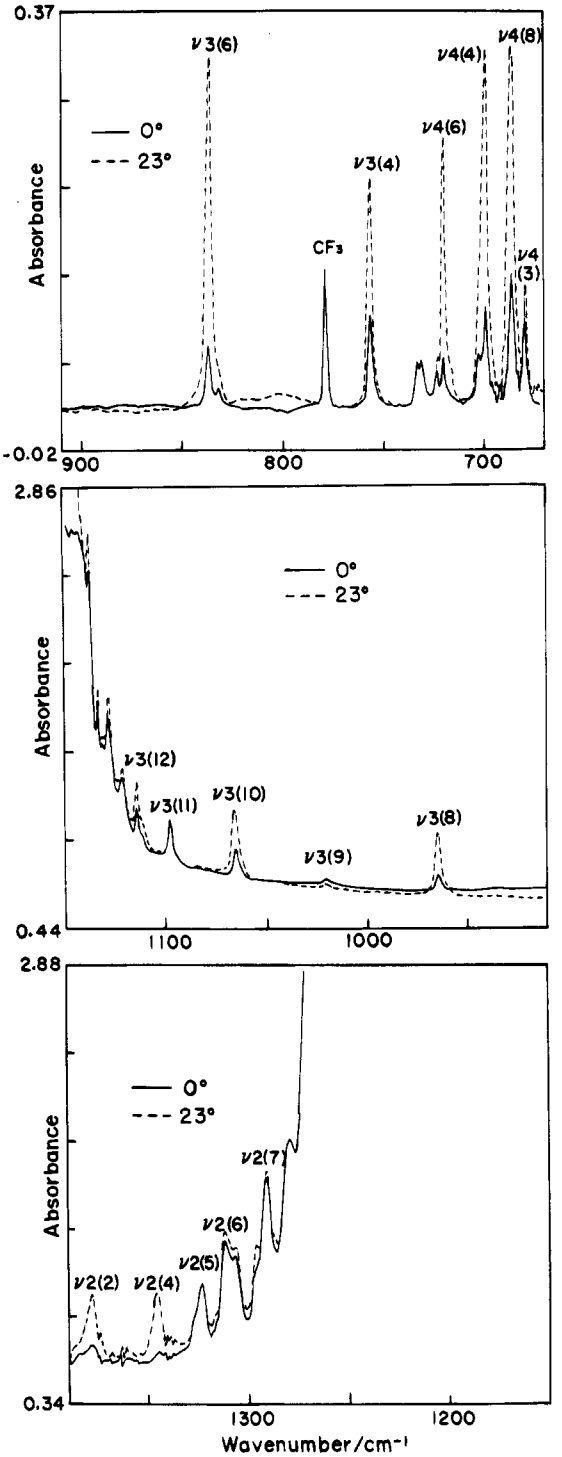

Figure 3. Infrared spectra of $C_{20}F_{42}$ single crystals at 110 K taken with the inclination angles of θ = 0° (solid lines) and θ = 23 ° (broken lines).

intense perpendicular bands caused by optical aberration, misalignment of the molecules, etc. or (2) one of them, e.g., the 1219 cm^{-1} band, is assigned to the $A_2(1)$ mode. At present, it is difficult to decide whether the $A_2(1)$ mode is assignable to the weak parallel component at 1219 cm^{-1} or to a very weak band around 1450 cm^{-1} measured in $C_{24}F_{50}$ (see Figure 5). In any case, the oscillator strength of the $A_2(1)$ mode is very small compared with the other A_2 modes. Therefore, the morphology-dependent frequency shift of this mode is predicted to be undetectably small.

Two different types of dispersion curves of PTFE were presented by previous authors. The difference is par-

Table 1. Frequencies and Assignments of Infrared Bands of $C_{20}F_{42}$

frequency at 299 K (cm^{-1})			frequency at 108 K (cm^{-1})			
powder	single crystal	thin film[a]	powder	single crystal	assignment	polarization
524	531	531	522	527	$A_2(3)$	(∥)
			530	531	$\nu_5(2)$	(∥)
542		546	540	543	$\nu_5(4)$	(∥)
555	555		553	553	$E_1(4)^d$	(⊥)
			558	558	$E_1(4)^d$	(⊥)
				562	$\nu_4(16)$	(⊥)
			570	570	$\nu_4(15)$	(⊥)
			576	580	$\nu_4(14)$	(∥)
			591	591	$\nu_4(13)$	(⊥)
601			601	601	$\nu_4(12)$	(∥)
			620	620	$\nu_4(11)$	(⊥)
630	633	632	632	632	$A_2(2)^b$	(∥)
			634	634	$\nu_4(10)$	(∥)
	648			646	$\nu_4(9)$	(⊥)
642		647	648	654	$A_2(2)^b$	(∥)
			679	680	$\nu_4(3)$	(⊥)
685	685	686	688	686	$\nu_4(8)$	(∥)
698	699	699	701	699	$\nu_4(4)$	(∥)
				702	$\nu_4(7)$	(⊥)
720	720	720	720	720	$\nu_4(6)$	(∥)
				723	$\nu_4(5)$	(⊥)
738	738		739	739	$A_1(2)$	Raman
				733	$\nu_3(2)$	(⊥)
747	747				$\nu_3(3)$	(⊥)
757	757	758	758	756	$\nu_3(4)$	(∥)
777	777		778	779	$\nu_s(CF_3)$	(⊥)
				832	$\nu_3(5)$	(⊥)
834	835	834	840	837	$\nu_3(6)$	(∥)
841	841	841			satellite of $\nu_3(6)$	
854	855	855			satellite of $\nu_3(6)$	
891	891				$\nu_3(7)$	(⊥)
961	962	962	967	965	$\nu_3(8)$	(∥)
969	967	967			satellite of $\nu_3(8)$	
1011	1011				$\nu_3(9)$	(⊥)
1063	1063	1063	1068	1066	$\nu_3(10)$	(∥)
1093	1093		1095	1097	$\nu_3(11)$	(⊥)
1111	1112	1111	1113	1114	$\nu_3(12)$	(∥)
1126			1125	1121	$\nu_3(13)$	(⊥)
		1125	1129	1128	$\nu_3(14)$	(∥)
			1134	1133	$\nu_3(15)$	(⊥)
		1138	1140	1137	$\nu_3(16)$	(∥)
			1145		$\nu_3(17)$	(⊥)
1157	*c*	1155	1155	*c*	$E_1(3)$	(⊥)
			1170		$\nu_2(12)$	(⊥)
			1188		$\nu_2(14)$	(⊥)
1216	*c*	1219	1211	*c*	$E_1(2)$	(⊥)
1230	*c*		1235	*c*	$E_1(1)$	(⊥)
		1254				
				1279	$\nu_2(8)$	(⊥)
		1288				
	1297		1296	1291	$\nu_2(7)$	(⊥)
	1313		1311	1306	$\nu_2(6)$	(⊥)
				1323	$\nu_2(5)$	(⊥)
1340	1341	1340	1346	1345	$\nu_2(4)$	(∥)
1373	1374	1374	1378	1377	$\nu_2(2)$	(∥)
1379			1379		$A_1(1)$	Raman

[a] Measured by RAS. [b] Fermi resonance doublet. [c] Not observed due to saturation. [d] Davydov split in the monoclinic phase.

ticularly notable for the ν_1 and ν_2 branches. In the present work, the dispersion curves were examined based on the spectral data of the progression bands (Figure 4). If the $A_2(1)$ mode is assigned to the band around 1450 cm^{-1} (case 1), the ν_1 starts at the point (ν = 1450 cm^{-1}, $\phi = 0°$) and goes toward the $E_1(1)$ mode (ν = 1252 cm^{-1}, $\phi = 168°$). There are no observed data points between these two points. The ν_2 starts at the $A_1(1)$ mode (ν = 1379 cm^{-1} as observed in Raman spectrum, $\phi = 0°$) and goes toward the $E_1(2)$ mode (ν = 1206 cm^{-1}, $\phi = 168°$) with many progression bands in between. The ν_3 starts at the $A_1(2)$ mode (ν = 738 cm^{-1}

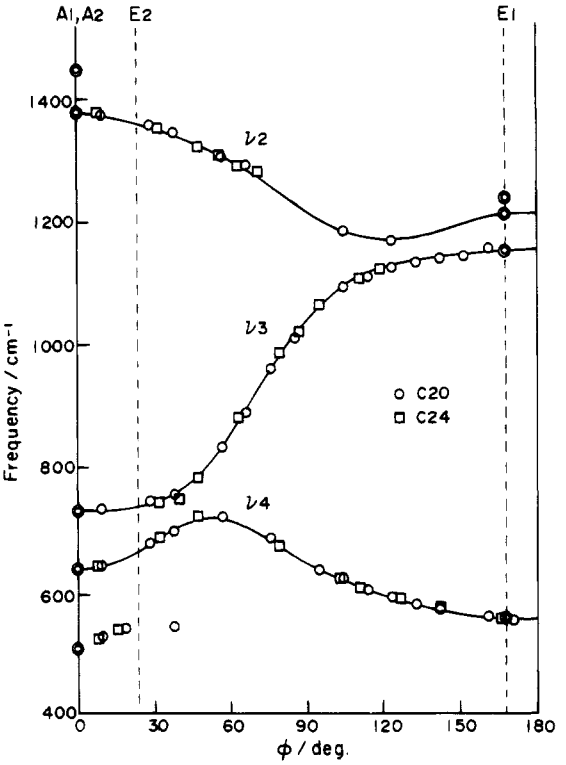

Figure 4. Dispersion curves of the ν_2, ν_3, and ν_4 branches derived from the observed frequencies of the progression bands of $C_{20}F_{42}$ (○) and $C_{24}F_{50}$ (□) along with the zone-center modes of PTFE (◎). The phase angles of the A_1, A_2, E_1, and vibrations of PTFE are indicated.

as observed in the Raman spectrum, $\phi = 0°$) and goes toward the $E_1(3)$ mode (ν = 1151 cm^{-1}, $\phi = 168°$) with many data points in between. The steepest slope of the dispersion around $\phi = 70°$ is rather close to the result calculated by Hannon et al.[19] On the contrary, if the $A_2(1)$ mode is assigned to the weak parallel component at 1219 cm^{-1} (case 2), the ν_1 starts at the $A_1(1)$ mode and goes toward the $E_1(1)$ mode. This corresponds to the ν_2 branch of case 1, except for the region around ϕ = 160°. The ν_2 starts at the $A_2(1)$ mode and goes toward the $E_1(2)$ mode. Because of the very small frequency gap between these two modes, no progression bands on this branch are detected. At present, it is difficult to conclude which case is more reliable. In Figures 3, 4, and 13 as well as in Table 1, we adopt conventionally the notation of the branches defined in case 1.

Frequencies and Absorption Profiles of the A_2 Bands in Relation to the Crystal Morphology

In Figure 5 unpolarized IR spectra taken on powder samples of emulsion-polymerized PTFE (P1), $C_{20}F_{42}$, and $C_{24}F_{50}$ are compared with one another. In the P1 sample having an ECC-type morphology, the $A_2(2)$ and $A_2(3)$ bands appear, respectively, at 636 and 505 cm^{-1}, while they are shifted to 642 and 524 cm^{-1} in the lamellar crystals of the oligomers. On the contrary, the E_1 bands as well as the Raman-active A_1 bands (Figure 6) appear at the same positions within the experimental ambiguity in these three samples.

The spectral profiles of the A_2 bands are influenced by the state of the sample. In Figure 7 are shown the IR spectra of $C_{20}F_{42}$ in the 700–490 cm^{-1} region containing the $A_2(2)$, $A_2(3)$, and $E_1(4)$ bands in three different crystalline states (at room temperature): a polycrystalline powder, a single crystal with the basal normal inclined by 30° to the incident radiation for

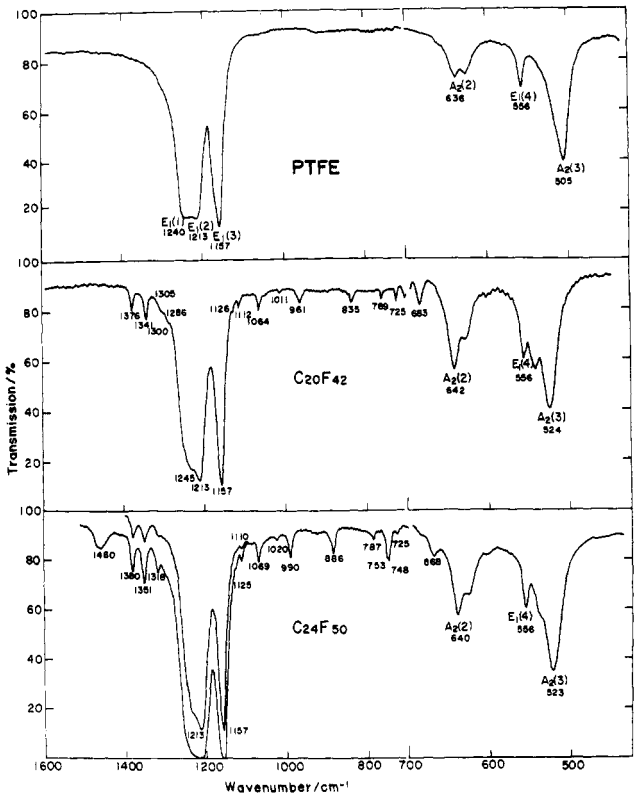

Figure 5. Infrared spectra of powder samples of PTFE (P1), $C_{20}F_{42}$, and $C_{24}F_{50}$.

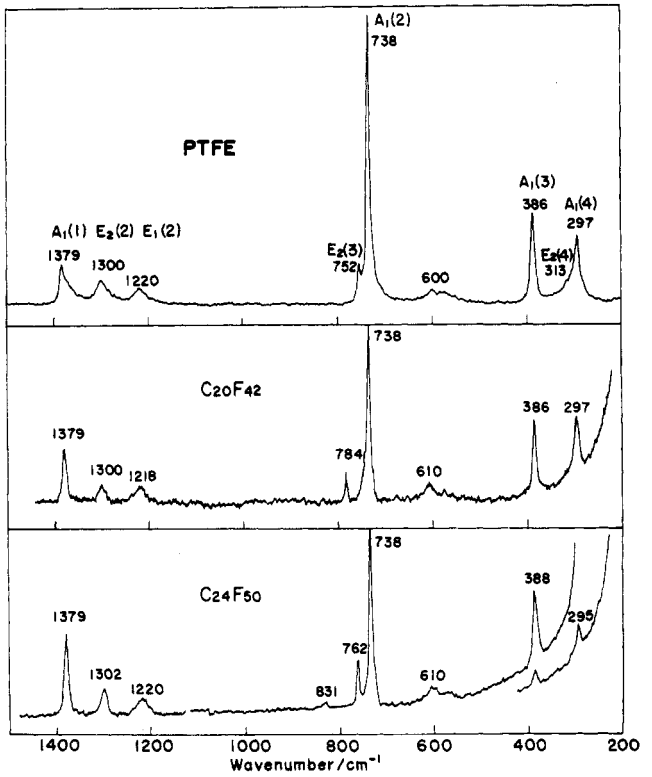

Figure 6. Raman spectra of powder samples of PTFE (P1), $C_{20}F_{42}$, and $C_{24}F_{50}$.

observing the parallel bands, and a thin film deposited on an aluminum plate measured by RAS. In Figure 7a, the absorption profiles in the 590–490 cm^{-1} region are divided into five Lorentzian components after the correction of the base line (the broken lines). The highest component at 555 cm^{-1} is due to the $E_1(4)$ perpendicular band (hence, it disappears in the RAS) and the other

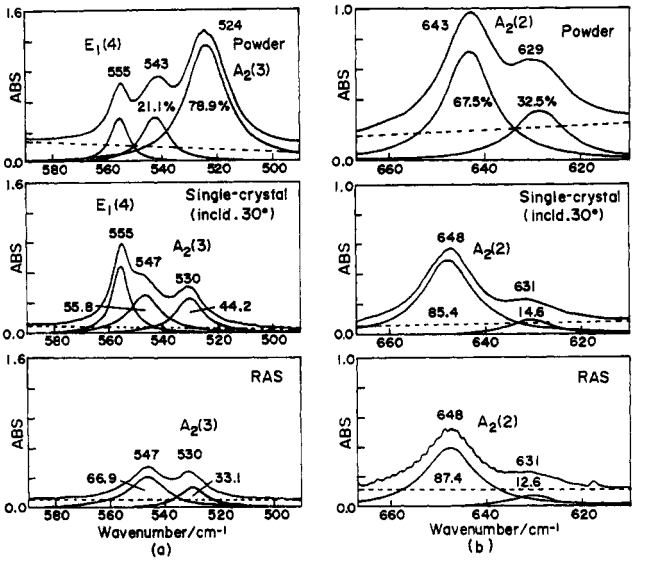

Figure 7. Infrared absorption profiles of $C_{20}F_{42}$ in three different crystalline states: powder, single crystal, and thin film deposited on an aluminum plate (measured by RAS).

two are due to the $\nu_5(1)$ [i.e., $A_2(3)$] and $\nu_5(2)$ bands with parallel polarization. The relative integrated intensities (in percent) of the parallel absorptions are described in the figure. The peak position of the $A_2(3)$ band is further shifted toward the high-frequency side as the sample goes from polycrystalline to the well-grown lamellar type. At the same time, the intensity distribution between the $\nu_5(1)$ and $\nu_5(2)$ components varies. Contrary to the significant change of these parallel bands, the $E_1(4)$ perpendicular band does not show any change in either frequency or profile.

The similar spectral change of the parallel bands in the 670–610 cm^{-1} region is shown in Figure 7b. Before discussing the spectral characteristics, we have to mention the assignment of the $A_2(2)$ band in PTFE. In the IR spectrum of PTFE, there appears a doublet with peaks at 639 and 626 cm^{-1}. The former has been assigned to the $A_2(2)$ mode [approximately, the CF_2 wagging: w(CF_2)] of the (15/7) or (13/6) helix, and the latter to the corresponding local mode associated with *trans* sequences formed in the helix as a result of the helix reversal motion, on the basis of the experimental fact that it becomes stronger with increasing temperature and also of the calculated density of states for a PTFE molecule containing such type of conformational defects.[22]

However, we propose another interpretation for the doublet. As shown in Figures 5 and 7b, the absorption profile at a constant temperature (at 25 °C) is influenced by the state of the sample not only in the relative intensity but also in the peak positions. The integrated intensity ratio $R = A_{high}/A_{low}$ of the doublet varies as follows: $R = 50/50$ for P1, $R = 68/32$ for polycrystalline $C_{20}F_{42}$, $R = 85/15$ for single-crystal $C_{20}F_{42}$, and $R = 87/13$ for thin-layer $C_{20}F_{42}$. The peak positions are shifted toward the high-frequency side in this order. We consider that the spectral change should be explained by the Fermi resonance between the $A_2(2)$ fundamental mode and the $E_1(5)$ (383 cm^{-1}) × $E_1(6)$ (278 cm^{-1}) combination mode. The frequencies of the $E_1(5)$ and $E_1(6)$ modes were measured by far-infrared spectroscopy (Figure 8). Since the combination includes the A_2 species ($E_1 \times E_1 = A_1 + A_2 + E_2$), it is able to couple with the $A_2(2)$ fundamental, giving rise to a doublet through the Fermi resonance. The absorption due to

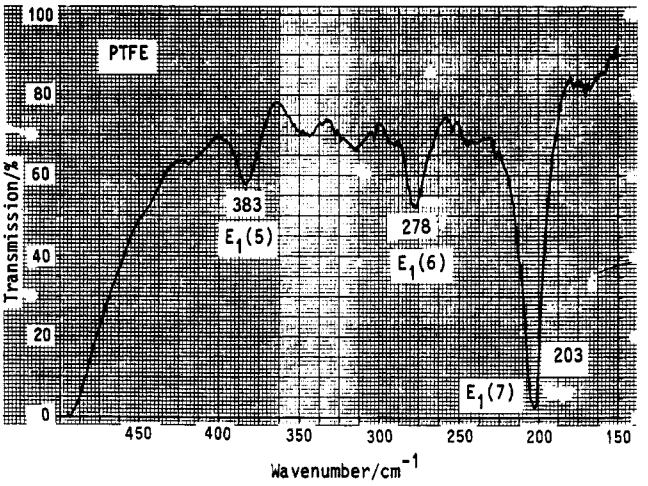

Figure 8. Far-infrared spectrum of PTFE.

Table 2. Morphology-Dependent Band Shifts (cm^{-1}) of the A_2 Modes of PTFE

sample	$A_2(2)$ mode				$A_2(3)$ mode
PTFE (P1)	639	(50.0:50.0)[a]	629	634.0	505
$C_{20}F_{42}$ (powder)	643	(67.5:32.5)	629	638.4	520
$C_{20}F_{42}$ (single crystal)	648	(85.4:14.6)	631	645.5	530
$C_{20}F_{42}$ (thin film)	648	(87.4:12.6)	631	645.8	530

[a] The integrated intensity ratio of the Fermi resonance doublet is given in parentheses.

the Fermi resonance doublet varies very sensitively with the position of the $A_2(2)$ fundamental, which moves with change in crystal morphology. In other words, the morphology-dependent spectral change is enhanced by Fermi resonance. From the measured peak positions and the intensity ratio of the doublet components, the intrinsic values of the $A_2(2)$ mode frequency for the respective samples were evaluated as summarized in Table 2, where also the $A_2(3)$ mode frequencies are given.

A_2 Band Shifts Predicted by Transition Dipolar Coupling Theory

As reported in ref 8, the magnitude of the band shift (in cm^{-1}) for the kth fundamental is expressed by the equation

$$\Delta\nu_k(0\rightarrow 1) = (1/8\pi^2c^2\nu_k^0)(\partial\mu/\partial Q_k)_0^2\sum(K_j/R_j^3) \quad (2)$$

where μ denotes the dipole moment of the whole crystallite, Q_k the normal coordinate of the kth mode, and ν_k^0 the intrinsic frequency (in cm^{-1}) of the kth mode free from the transition dipolar interactions. $\sum(K_j/R_j^3)$ is the geometric factor (the Madelung constant) related to the spatial distribution of the transition dipole moments within the whole crystallite. Each K_j/R_j^3 term for the interaction between the transition dipoles at the origin (the 0th dipole) and the jth one is expressed by the following equation using the parameters defined in Figure 9:

$$K_j/R_j^3 = (\cos\theta_{0,j} - 3\cos\theta_0\cos\theta_j)/R_j^3 \quad (3)$$

Since the IR parallel bands arise from the in-phase oscillation of the transition dipoles along the chain axis,

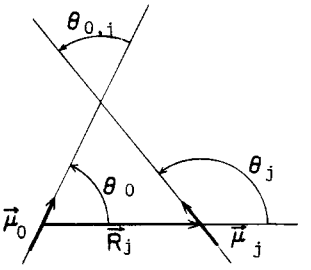

Figure 9. Dipole–dipole interaction.

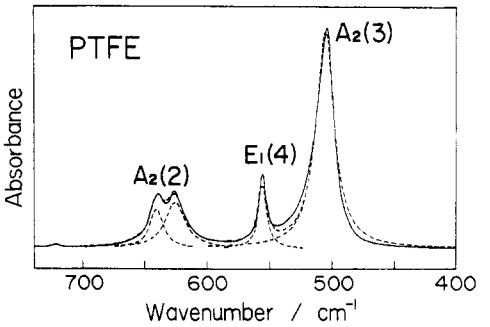

Figure 10. Separation of infrared absorption profile of PTFE (P1) in the 700–400 cm^{-1} region.

the geometric factor for the parallel bands is reduced to

$$\sum(K_j/R_j^3) = \sum(1 - 3\cos^2\theta_j)/R_j^3 \quad (4)$$

In ref 8, it has been shown that the magnitude of the geometric factor vanishes for the extreme case of the ideal ECC and increases monotonously as the crystal morphology goes to the lamellar type (see Figure 12 in ref 8), approaching the maximum for the ideal lamellar crystal, i.e., for the two-dimensional lattice. For such a two-dimensional lattice, the geometric factor becomes $\sum(1/R_j^3)$ whose value for PTFE is obtained as 0.0484 $Å^{-3}$ from the hexagonal lattice determined by Bunn and Howells.[13]

$(\partial\mu/\partial Q_k)_0^2$ in eq 2 is expressed in terms of the integrated molar absorption coefficient A ($cm\ mol^{-1}$) as

$$(\partial\mu/\partial Q_k)_0^2[\text{in cm}^3\ \text{s}^{-1}] = 3c^2A/N_A\pi = 1.426\times 10^{-3}A \quad (5)$$

where c ($cm\ s^{-1}$) denotes the velocity of light in a vacuum and N_A is the Avogadro constant. The values of A for the $A_2(2)$ and $A_2(3)$ modes in the absolute scale were obtained as follows. IR spectra of the powder P1 sample were measured on KBr pellets of various polymer concentration c_p. The thickness d of each pellet was measured using a dial gauge. The absorption profile in the 700–400 cm^{-1} range was separated into four Lorentzian curves as shown in Figure 10. The integrated intensities I of the $A_2(2)$ (the doublet caused by the Fermi resonance), $A_2(3)$, and $E_1(4)$ bands were obtained. The A value of each mode was evaluated from the slope of the I/d vs c_p line as shown in Figure 11. The magnitudes of oscillator strength A/ν_k^0 (in $cm^2\ mol^{-1}$) per monomeric unit were obtained as given in Table 3.

The maximum frequency gap for the kth mode between the ideal ECC and lamellar morphologies is derived from eq 2 as

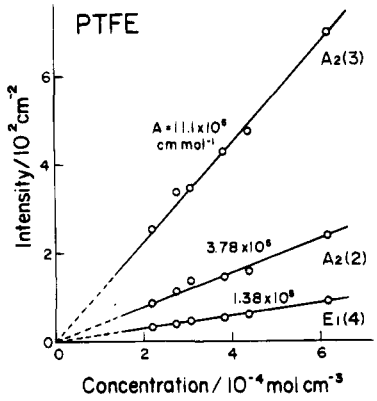

Figure 11. Integrated intensities (per unit thickness of KBr pellet) of the $A_2(2)$, $A_2(3)$, and $E_1(4)$ bands of PTFE as a function of polymer concentration. The values of the integrated molar absorption coefficients A are indicated.

Table 3. Calculated and Observed Frequency Shifts of the Infrared Parallel Bands of PTFE

mode	ν^0 (cm^{-1})	A ($cm\ mol^{-1}$)	A/ν^0 ($cm^2\ mol^{-1}$)	$\Delta\nu_{calc}$ (cm^{-1})	$\Delta\nu_{obs}$ (cm^{-1})
$A_2(2)$	634	3.78×10^5	5.96×10^2	8.7	12
$A_2(3)$	505	11.1×10^5	2.20×10^3	32.1	25

$$\Delta\nu_k^{M}[\text{in cm}^{-1}] = (1/8\pi^2c^2)(A/\nu_k^0)(\sum R^{-3}) = 2.009 \times 10^{-2} p(A/\nu_k^0)[\text{in cm}^2\ \text{mol}^{-1}](\sum R^{-3})[\text{in Å}^{-3}] \quad (6)$$

where p denotes the number of monomeric units that consist of the unit transition dipole (in the point dipole approximation).

The values for the $A_2(2)$ and $A_2(3)$ modes were calculated as given in Table 3, in good agreement with the experimental $\Delta\nu_k$ values measured between the PTFE whisker (P1) and the thin layer of $C_{20}F_{42}$ deposited on an aluminum plate (see Table 2). Here we assume that one unit transition dipole consists of 15 CF_2 groups, i.e., $p = 15$.

The IR perpendicular bands assignable to the doubly degenerate species do not show such morphology-dependent frequency shifts, because the transition dipolar interactions are canceled out when they are summed up over the whole crystallite.[8,24] The IR-inactive Raman bands are not influenced by the crystal morphology simply because $(\partial\mu/\partial Q_k)_0^2 = 0$.

Transition Dipolar Interactions in Mixed Crystals of $C_{20}F_{42}$ and $C_{24}F_{50}$

As described in the preceding section the high-frequency shifts of the IR parallel bands are caused by the in-phase oscillation of the parallel transition dipoles among the molecules constructing a single domain of the lamellar crystallite. If such an in-phase relation among the neighboring molecules in the lamellar crystallie is destroyed by some causes, the high-frequency shifts might cease to occur. In fact, this was confirmed experimentally for lamellar-type mixed crystals of normal and deuterated paraformaldehydes (PFA and PFA-d_2, linear oligomers of POM and POM-d_2) where the in-phase oscillation is hampered by different normal frequencies of the mutually surrounding two isotopic species.[27] The result showed that PFA-d_2 molecules surrounded by PFA molecules in solution-grown lamellar-type mixed crystals gave rise to the parallel A_2 bands at the frequencies free from the transition dipolar interactions.

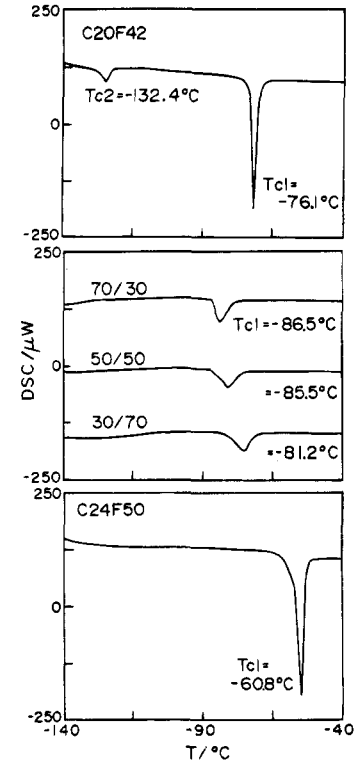

Figure 12. DSC thermograms (on heating) of $C_{20}F_{42}$ and $C_{24}F_{50}$ and their mixed crystals with different compositions (indicated by the mole ratio $C_{20}F_{42}/C_{24}F_{50}$).

A similar effect caused by the disturbance of the in-phase oscillation is anticipated in mixed crystals of linear oligomers having different chain lengths. In this case, the in-phase oscillation is maintained for the most-in-phase modes (i.e., the modes with $k = 1$ in eq 1 for the parallel bands), because their frequencies are almost independent of the chain length and approximately identical with those of the corresponding zone-center A_2 modes. Therefore, the parallel most-in-phase bands in the mixed crystals should exhibit the same morphology-dependent shifts as those in pure $C_{20}F_{42}$ or $C_{24}F_{50}$ crystals. On the contrary, the frequencies of the other progression bands depend on the chain length. Therefore, the transition dipolar interactions for these bands should be reduced in the mixed crystals.

Mixed crystals of $C_{20}F_{42}$ and $C_{24}F_{50}$ prepared in the present work (see Experimental Section) are represented here by the mole ratio $C_{20}F_{42}/C_{24}F_{50}$. They give rise to DSC thermograms (on heating) shown in Figure 12 in comparison with those of pure $C_{20}F_{42}$ (upper) and $C_{24}F_{50}$ (bottom). In every mixed crystal, there appears one broad endothermic peak at a temperature lower than the transition temperature of $C_{20}F_{42}$ from the intermediate phase to the rhombohedral phase,[10] indicating that $C_{20}F_{42}/C_{24}F_{50}$ cocrystals are formed in our samples. The IR spectra of these cocrystals were measured at various temperatures down to 100 K.

The IR spectrum of the (25/75) mixed crystal measured at 110 K is reproduced in Figure 13 in comparison with the weighted superposition of the spectra of pure $C_{20}F_{42}$ and $C_{24}F_{50}$ measured at the same temperature (broken lines). Assignments of the $\nu_3(k)$ progression bands associated with $C_{20}F_{42}$ and $C_{24}F_{50}$ are indicated on the figure. The $\nu_3(k)$ bands due to $C_{20}F_{42}$ (the minor component) in the mixed crystal are red-shifted from the positions of pure $C_{20}F_{42}$. The $\nu_3(k)$ bands due to $C_{24}F_{50}$ (the major component) show similar but less pronounced red shifts. The results obtained for mixed

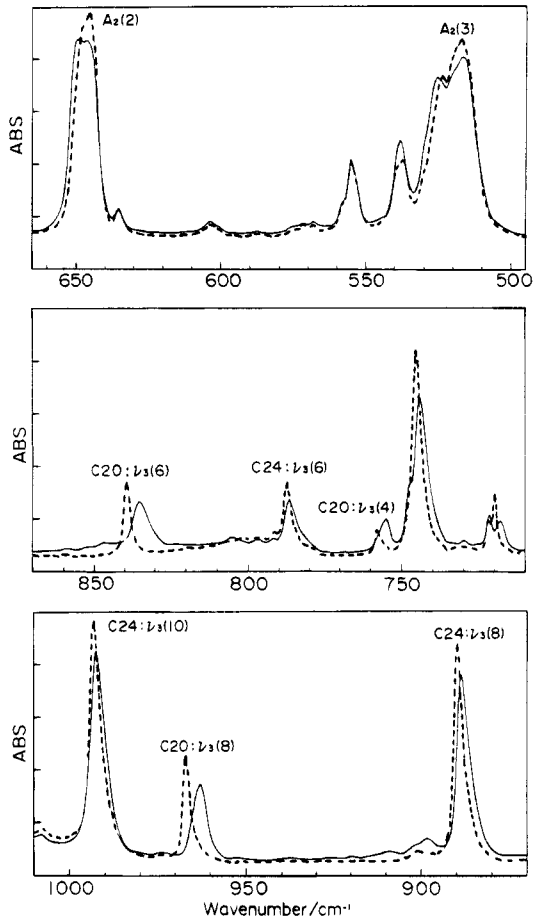

Figure 13. Infrared spectra of the (25/75) mixed crystal measured at 110 K (solid lines) in comparison with the weighted superposition of the spectra of pure $C_{20}F_{42}$ and $C_{24}F_{50}$ (in the powder state) measured at 110 K (broken lines).

Table 4. Frequency Shifts (cm^{-1}) of the $\nu_3(k)$ Progression Bands of $C_{20}F_{42}$ and $C_{24}F_{50}$ in Their Mixed Crystals with Various Mole Ratios ($C_{20}F_{42}/C_{24}F_{50}$) Measured at 110 K

	mole ratio							
	100/0	80/20		55/45		25/75		0/100
mode	ν	ν	$\Delta\nu$	ν	$\Delta\nu$	ν	$\Delta\nu$	ν
				$C_{20}F_{42}$ Component				
$\nu_3(4)$	758.1	757.9	−0.2	756.7	−1.4	755.0	−3.1	
$\nu_3(6)$	839.6	838.9	−0.7	837.5	−2.1	835.0	−4.6	
$\nu_3(8)$	966.9	966.5	−0.4	965.3	−1.6	962.8	−4.1	
$\nu_3(10)$	1067.3	1067.0	−0.3	1066.3	−1.0	1065.3	−2.0	
				$C_{24}F_{50}$ Component				
$\nu_3(4)$		742.9	−2.7	743.9	−1.7	744.4	−1.2	745.6
$\nu_3(6)$				786.8	−0.6	786.8	−0.6	787.5
$\nu_3(8)$		888.3	−1.5	888.6	−1.2	888.8	−1.0	889.8
$\nu_3(10)$		992.5	−0.7	992.7	−0.5	992.7	−0.5	993.2
$\nu_3(12)$		1071.1	−0.7	1071.4	−0.4	1071.4	−0.4	1071.8

crystals of different compositions are summarized in Table 4. The magnitude of the red shift for a particular $\nu_3(k)$ band of one constituent increases with a decrease of its concentration (i.e., with increasing extent of dilution with the other constituent) as predicted from the transition dipolar coupling theory. The most-in-phase parallel bands [corresponding to the $A_2(2)$ and $A_2(3)$ fundamentals of PTFE] remain unshifted in the mixed crystal regardless of the composition.

The transition dipolar coupling theory also predicts that the magnitude of the red shift in the mixed crystals is more pronounced for the progression band which has greater oscillator strength and is positioned more distant from any one of the progression bands due to the diluent molecules. In fact, the largest red shift is observed for the $\nu_3(6)$ band of $C_{20}F_{42}$, which has a comparatively large oscillator strength and is well separated from both the $\nu_3(6)$ and $\nu_3(8)$ bands of $C_{24}F_{50}$. The $\nu_3(8)$ band of $C_{20}F_{42}$ has a larger oscillator strength than the $\nu_3(6)$ band but locates rather close to the $\nu_3(10)$ band of $C_{24}F_{50}$. Consequently, the $\nu_3(6)$ and $\nu_3(8)$ bands are red-shifted by nearly the same magnitude.

Acknowledgment. The authors thank Daikin Industrial Ltd. for kindly supplying the PTFE samples.

References and Notes

(1) Shimomura, M.; Iguchi, M. *Polymer* **1982**, *23*, 509.
(2) Shimomura, M.; Iguchi, M.; Kobayashi, M. *Polymer* **1988**, *29*, 351.
(3) Shimomura, M.; Iguchi, M.; Kobayashi, M. *Polymer* **1990**, *31*, 1406.
(4) Kobayashi, M.; Sakashita, M.; Hasegawa, M. *Macromolecules* **1991**, *24*, 4796.
(5) Kobayashi, M.; Morishita, H.; Shimomura, M. *Macromolecules* **1989**, *22*, 3726.
(6) Kobayashi, M.; Gu, Q.; Kaneko, F.; Iguchi, M.; Shimomura, M. *Polym. Prepr. Jpn.* **1984**, *33*, 2089.
(7) Shimomura, M.; Tanabe, Y.; Watanabe, Y.; Kobayashi, M. *Polymer* **1990**, *31*, 1411.
(8) Kobayashi, M.; Sakashita, M. *J. Chem. Phys.* **1992**, *96*, 748.
(9) Folda, T.; Hoffmann, H.; Chanzy, H.; Smith, P. *Nature* **1988**, *333*, 55.
(10) Schwickert, H.; Strobl, G.; Kimmig, M. *J. Chem. Phys.* **1991**, *95*, 2800.
(11) Wittmann, J. C.; Smith, P. *Nature* **1991**, *352*, 414.
(12) Montamedi, F.; Ihn, K. J.; Fenwick, D.; Wittmann, J. C.; Smith, P. *J. Polym. Sci., Part B: Polym. Phys.* **1994**, *32*, 453.
(13) Bunn, C. W.; Howells, E. R. *Nature* **1954**, *174*, 549.
(14) Clark, E. S.; Muus, L. T. *Z. Kristallogr.* **1962**, *117*, 119.
(15) Kilian, H. G. *Kolloid Z.* **1962**, *185*, 13.
(16) McCall, D. W.; Douglass, D. C.; Falcone, D. R. *J. Phys. Chem.* **1967**, *71*, 998.
(17) Linag, C. Y.; Krimm, S. *J. Chem. Phys.* **1956**, *25*, 563.
(18) Moynihan, R. E. *J. Am. Chem. Soc.* **1959**, *81*, 1045.
(19) Hannon, M. J.; Boerio, F. J.; Koenig, J. L. *J. Chem. Phys.* **1969**, *50*, 2829.
(20) Piseri, L.; Powell, B. M.; Dolling, G. *J. Chem. Phys.* **1973**, *58*, 158.
(21) Boerio, F. J.; Koenig, J. L. *J. Chem. Phys.* **1970**, *52*, 4826.
(22) Rabolt, J. F.; Fanconi, B. *Macromolecules* **1978**, *11*, 740.
(23) Hsu, S. L.; Reynolds, N.; Bohan, S. P.; Strauss, H. L.; Snyder, R. G. *Macromolecules* **1990**, *23*, 4565.
(24) Zerbi, G.; Sacchi, M. *Macromolecules* **1973**, *6*, 692.
(25) Masetti, G.; Cabassi, F.; Morelli, G.; Zerbi, G. *Macromolecules* **1973**, *6*, 700.
(26) Hexter, R. M. *J. Chem. Phys.* **1962**, *36*, 2285.
(27) Kobayashi, M.; Matsumoto, Y. *Rep. Prog. Polym. Phys. Jpn.* **1993**, *36*, 401.

MA941056E